

Article

Discrete Sliding Mode Control Strategy for Start-Up and Steady-State of Boost Converter

Tao Yang *  and Yong Liao

State Key Laboratory of Power Transmission Equipment & System Security and New Technology, Chongqing University, Chongqing 400044, China

* Correspondence: 20121101011@cqu.edu.cn

Received: 25 June 2019; Accepted: 30 July 2019; Published: 2 August 2019



Abstract: Since the zero initial conditions of the boost converter are far from the target equilibrium point, the overshoot of the input current and the output voltage will cause energy loss during the start-up process when the converter adopts the commonly used small-signal model design control method. This paper presents a sliding mode control strategy that combines two switching surfaces. One switching surface based on the large-signal model is employed for the start-up to minimize inrush current and voltage overshoot. The stability of this strategy is verified by Lyapunov theory and simulation. Once the converter reaches the steady-state, the other switching surface with PI compensation of voltage error is employed to improve the robustness. The latter switching surface, which is adopted to regulate the voltage, can not only suppress the perturbation of input voltage and load, but also achieve a better dynamic process and a zero steady-state error. Furthermore, the discrete sliding mode controller is implemented by digital signal processor (DSP). Finally, the results of simulation, experiment and theoretical analysis are consistent.

Keywords: boost converter; sliding mode control; start-up; target equilibrium point; voltage regulation

1. Introduction

Nowadays, the research of renewable energy is increasing due to energy shortages and pressure to reduce greenhouse gas emissions [1]. Power converters play an important role in renewable energy conversion [2]. Fuel cell hybrid electric vehicles need a DC–DC boost converter to suppress the variations of the fuel cell output voltage [3,4]. The nonlinearity of the boost converter is an obstacle when we analyze its characters [5–7]. To overcome this problem, a linear model of the boost converter should be built. The state-space averaging method is a commonly used linear modeling method, that is, its linear small-signal model is established around the steady-state operating point [8]. However, in the start-up process, the initial value of output voltage and the initial value of input current are both equal to zero and there is a large deviation from the target equilibrium point. The inrush current and voltage overshoot occur during the start-up process. Moreover, there is a nonminimum phase phenomenon in the control method of a boost converter based on the small-signal model. Therefore, it is impossible to deal with the system parameter changes and large-signal transient caused by start-up or load changes [9–11].

In a practical application, the sliding mode control (SMC) has the advantages of a fast dynamic response, good stability and strong anti-disturbance ability [12–14]. A grid voltage observer based on a sliding mode is proposed in [15] and verified by experiments. The basic positive and negative sequences can be accurately estimated and separated for voltage sensorless operation in an unbalanced network. An extended Luenberger-sliding mode observer is proposed in [16], which can estimate the rotor flux and resistance along with the adaptation method to compensate for the error caused by

the mismatch between the motor parameter and the model in the controller. A novel adaptive-gain sliding mode observer is proposed in [17], which can improve the precision of sensorless control of permanent magnet linear synchronous motors. In [18], an improved sliding controller design method for the photovoltaic system is proposed, which can alleviate the disturbance caused by irradiance change and oscillation in large capacity voltage. Moreover, the controller designed by the improved method can drive photovoltaic voltage to accurately track MPPT reference value obtained from external calculation. For the quadratic boost converter, a sliding-mode controller based on a fixed-frequency pulse-width modulation (PWM) is proposed in [19]. A feed-forward control technique is proposed in [20] to improve the steady-state performance of the DC–DC asymmetric Multistage Stacked Boost Architecture converter. A sliding mode controller of the boost converter based on a robust pulse-width modulation is proposed in [21], which supplies power to constant power load in typical DC micro-grid. The methods of [19–21] do not consider the start-up situation and are only suitable for the steady-state.

The inrush current or voltage overshoot occurs in many power electronic converters during the start-up process. An input-adaptive boost converter that can start up by itself is proposed in [22], which has the advantages of strict input regulation and high efficiency. However, due to many passive devices in a boost converter, the efficiency is reduced. The inrush current analysis is given in [23,24], where the auxiliary diode and inductor of a boost converter are connected in parallel to obtain the minimum inrush current. However, although the inrush current can be reduced by an auxiliary diode branch, high du/dt happens in the filter capacitor, which may damage the components and devices.

Based on the analysis given above, a sliding mode control method combining two switching surfaces is proposed for different operating conditions of the boost converter in the start-up and the steady-state in this paper. The first switching surface is based on the big-signal model for start-up processes, to reduce the inrush current and voltage overshoot. The second surface with the PI controller is adopted to regulate the output voltage and suppress the perturbation of the input voltage and load when the boost converter is in the steady-state.

The rest of this paper is arranged as follows. In Section 2, the first switching surface $S_1(t)$ is proposed in the start-up process of the boost converter, and its stability is analyzed. In Section 3, the other switching surface $S_2(t)$ is proposed to regulate the output voltage in the steady-state. After that, the proposed discrete sliding mode control strategy is implemented based on DSP in Section 4. Then the experimental results are shown and analyzed in Section 5. Finally, conclusions are summarized in Section 6.

2. Sliding Control Strategy for Start-Up

Figure 1a,b corresponds to the circuit states of the boost converter in the switching-on state and switching-off state of a switching tube VT, respectively. The corresponding Equations (1) and (2) of Figure 1a is as follows:

$$L \frac{di_L}{dt} = u_{in} \quad (1)$$

$$C \frac{du_o}{dt} = \frac{u_o}{R} \quad (2)$$

where L , i_L , u_{in} , C , u_o and R represent inductor, inductor current, input voltage, capacitor, output voltage and load resistance, respectively. The corresponding Equations (3) and (4) of Figure 1b is as follows:

$$L \frac{di_L}{dt} = u_{in} - u_o, \quad (3)$$

$$C \frac{du_o}{dt} = i_L - \frac{u_o}{R}. \quad (4)$$

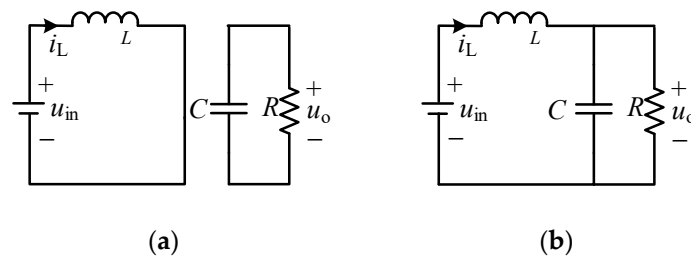


Figure 1. Circuit configurations of the boost converter in different switch state. (a) VT is switching-on. (b) VT is switching-off.

Variable p is defined as a switching state variable, if VT is switching-on, $p = 1$; else $p = 0$, the equations of boost converter can be expressed as:

$$L \frac{di_L}{dt} = u_{in} - (1 - p)u_o, \tag{5}$$

$$C \frac{du_o}{dt} = (1 - p)i_L - \frac{u_o}{R}. \tag{6}$$

2.1. Sliding Function for Start-Up

The average input power of the battery in one switching period is equal to the output power of load when the boost converter operates at a steady state. Ignoring the internal resistance and voltage drop of tube and diode, the relationship between i_L and u_o at steady-state is satisfied as follows:

$$i_L = \frac{u_o^2}{u_{in}R} u_o > u_{in}. \tag{7}$$

Due to $u_o > u_{in}$, the trajectory of Equation (7) is a part of a parabola. Define $S_1(t)$ as the switching surface for the start-up process, as shown below:

$$S_1(t) = I_L u_o(t) - U_o i_L(t). \tag{8}$$

(I_L, U_o) is the target equilibrium point satisfying Equation (7) at steady-state. I_L and U_o represent the inductor current and output voltage at the target equilibrium point respectively. The sliding mode control law is shown as:

$$\begin{aligned} p &= 1 \text{ if } S_1(t) > 0 \\ p &= 0 \text{ if } S_1(t) < 0 \end{aligned} \tag{9}$$

Figure 2 shows the sliding mode control model for start-up process, i_L and u_o are detected in the sampling period and substitute into Equation (8), so S_1 can be obtained. Finally, the switching signal of VT is generated by Equation (9).

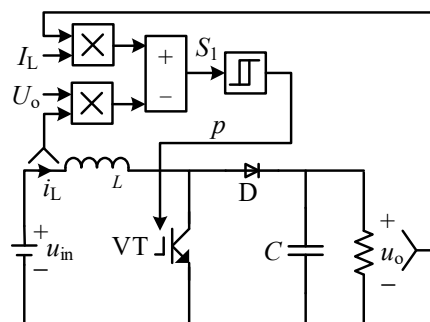


Figure 2. The sliding-mode control model for the start-up process.

2.2. Stability Analysis of the Sliding Function

Define the Lyapunov function as follows:

$$P = \frac{1}{2}S_1^2, \quad (10)$$

where the derivative of P is:

$$\dot{P} = S_1 \cdot \dot{S}_1. \quad (11)$$

According to Equations (5), (6) and (8), the expression of \dot{S}_1 can be obtained:

$$\dot{S}_1 = \frac{I_L}{C}(i_L - pi_L - \frac{u_o}{R}) - \frac{U_o}{L}(u_{in} - u_o + pu_o). \quad (12)$$

According to Equation (9), if $S_1 > 0$, \dot{S}_1 can be rewritten as:

$$\dot{S}_1 = -\frac{I_L u_o}{RC} - \frac{u_{in} U_o}{L}. \quad (13)$$

Due to $u_o > u_{in} > 0$, so $\dot{S}_1 < 0$.

If $S_1 < 0$, \dot{S}_1 is:

$$\dot{S}_1 = \frac{I_L}{C}(i_L - \frac{u_o}{R}) - \frac{U_o}{L}(u_{in} - u_o). \quad (14)$$

According to the characteristics of voltage boost and current buck, $i_L > u_o/R$, so $\dot{S}_1 > 0$.

Based on the above analysis, regardless of the value of S_1 , $P\dot{P} < 0$ can be satisfied. Therefore, the proposed sliding mode control system is stable in this paper, i_L and u_o can move to the trajectory of S_1 from any initial state, then reach the equilibrium point (I_L, U_o) along the switching surface.

2.3. Simulation of the Sliding Mode Control Based on S_1 in the Start-Up Process

The parameters of the boost converter adopted in this paper are shown in Table 1, where the values of inductance and capacitance are satisfied as follows:

$$L > \frac{u_{in} D_{max}}{\Delta i_{Lmax} f_s}, \quad (15)$$

$$C > \frac{D_{max}}{R f_s \eta_{max}}, \quad (16)$$

where D_{max} is the max duty, f_s is switching frequency, Δi_{Lmax} is the max current ripple, and η_{max} is the max voltage ripple ratio. After setting $D_{max} = 0.8$, $\Delta i_{Lmax} = 0.5$ A, $\eta_{max} = 1\%$, $f_s = 10$ kHz, Equations (15) and (16), can get the range of L and C is $L > 1.9$ mH and, $C > 192$ μ F, respectively. In this paper, L take the value of 2 mH and C is set to 265 μ F.

Table 1. Main parameters for the boost converter in the simulation and experiment.

Parameters	Values
Input Voltage u_{in}	12 V
Input Inductance L	2 mH
Filter Capacitance C	265 μ F
Resistance Load R	50 Ω

The target equilibrium point is set as $I_L = 1.02$ A, $U_o = 24$ V. Figure 3a shows the trajectory from original point (0 A, 0 V) to the target equilibrium point (I_L, U_o) by Matlab. The motion process of i_L

and u_o is divided into two steps: Firstly, they deviate from T_{S1} and increase simultaneously until $u_o > u_{in}$; then they start to approach T_{S1} . After that, when they reach T_{S1} , they move along T_{S1} to the target equilibrium point (I_L, U_o) . Even if the initial point is not at the original point, i_L and u_o can still adjust to the target equilibrium point by S_1 . The trajectory from the initial point (2.5 A, 30 V) to the target equilibrium point is shown in Figure 3b.

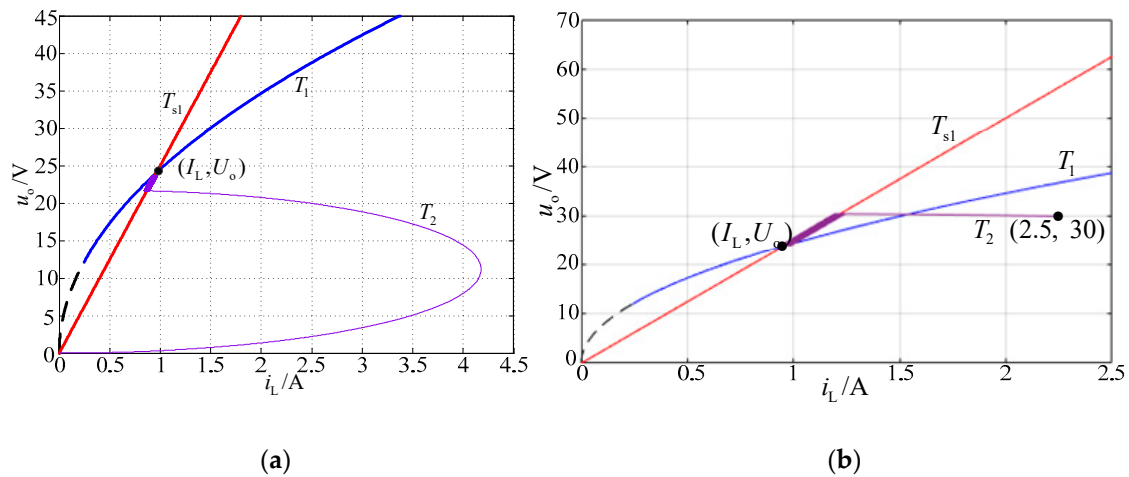


Figure 3. Start-up trajectory in the i_L - u_o plane. T_{S1} is the sliding curve of S_1 , T_1 is the trajectory of (7), T_2 is the tracking of the motion of i_L and u_o , respectively. (a) The initial point is (0 A, 0 V). (b) The initial point is (2.5 A, 30 V).

Figure 4a shows the simulation results of the control strategy based on the small-signal model in the start-up process. For comparison, Figure 4b shows the simulation results of the sliding mode control strategy proposed in this paper. In Figure 4a, the peak of i_L and u_o is corresponding to 5.86 A and 28.75 V, respectively. However, there is no voltage overshoot in Figure 4b, and the peak of i_L is only 4.12 A, which is lower than i_L shown in Figure 4a. Moreover, current discontinuation occurs in Figure 4a, therefore the time from the zero initial state to a steady state is much longer than Figure 4b. The results show that the sliding mode control of S_1 is correct and feasible.

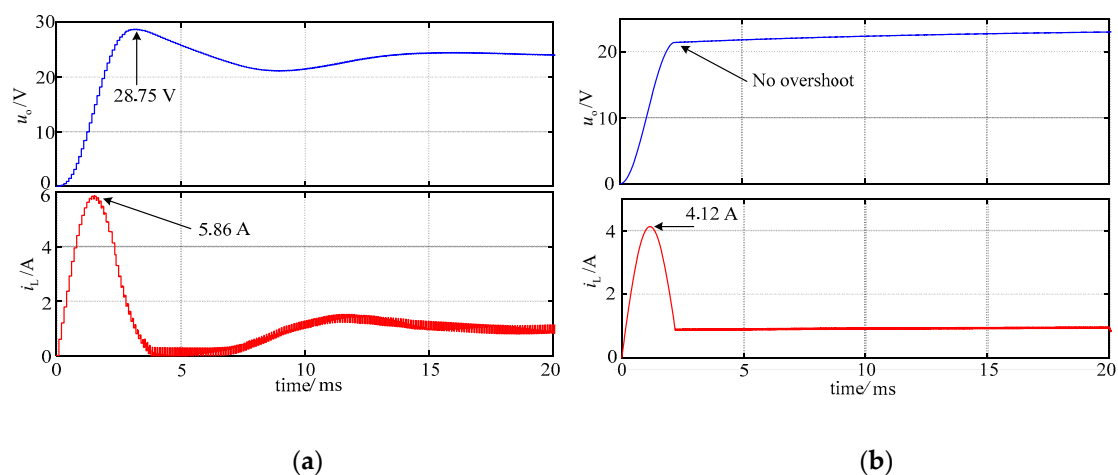


Figure 4. The simulation result of i_L and u_o in the start-up process. (a) Control based on the small-signal model. (b) Sliding control based on the big-signal model.

3. Voltage Control Strategy for Steady-State

Since the control strategy based on S_1 has a long time along the sliding line and poor robustness, it is only suitable for the start-up process. During steady-state, an error will occur when u_{in} or R

changes, therefore, another control strategy should be adopted to regulate the output voltage at this stage. Define switching surface $S_2(t)$ as follows:

$$S_2(t) = I_L + \Delta i_L(t) - i_L(t) \tag{17}$$

where Δi_L is current error compensation. When u_{in} or R is perturbed, if U_o is constant, the target equilibrium point changes from (I_L, U_o) to $(I_L + \Delta i_L, U_o)$. Δi_L can be expressed as

$$\Delta i_L(t) = k_p(U_o - u_o(t)) + k_i \int_{t_1}^{\infty} U_o - u_o(t) dt \tag{18}$$

where k_p is the proportional gain and k_i is the integral gain of the voltage PI controller. t_1 is the moment that the switching surface is switched from S_1 to S_2 . Substituting Equation (18) into Equation (17), $S_2(t)$ can be expressed as:

$$S_2(t) = I_L - i_L(t) + k_p(U_o - u_o(t)) + k_i \int_{t_1}^{\infty} U_o - u_o(t) dt. \tag{19}$$

The sliding control law of S_2 is shown as:

$$\begin{aligned} p &= 1 \text{ if } S_2(t) > 0 \\ p &= 0 \text{ if } S_2(t) < 0 \end{aligned} \tag{20}$$

Figure 5 shows the discrete sliding mode control model for steady-state. Δi_L is obtained by discrete PI operation of voltage error u_e , then the switching signal of VT is generated by Equation (20). z^{-1} is the delay unit, which is used to implement the discrete integral operation.

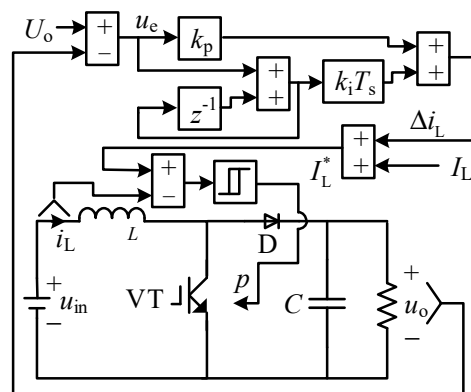


Figure 5. The discrete sliding mode control model for steady-state.

3.1. Analysis of Transient Process under Input Voltage Perturbations

Figure 6 shows the transient trajectory of i_L and u_o under different input voltage perturbations. The increase or decrease of u_{in} will lead to the deviation of the equilibrium point locus (EPL). Therefore, the steady-state equilibrium operating point will change from O (I_L, U_o) to Q (I_{LQ}, U_o) or P (I_{LP}, U_o). I_{LP} and I_{LQ} represent the inductor current at P and Q points respectively. When u_{in} steps from U_1 to U_3 ($U_1 > U_3$), (i_L, u_o) immediately move from initial equilibrium operating point O (I_L, U_o) to Q₁. The new reference value of i_L can be obtained by PI operation of voltage error and generates the VT switching signal according to the sliding control law of S_2 , makes i_L equal to I_{LQ} and u_o recovers to U_o correspondingly due to power conservation. A symmetrical situation will occur when u_{in} steps from

U_1 to U_2 . As shown in the same figure, the correction effects make i_L equal to I_{LP} . Along the trajectory $O \rightarrow P_1 \rightarrow P$, (i_L, u_o) reach to the new equilibrium point $P (I_{LP}, U_o)$.

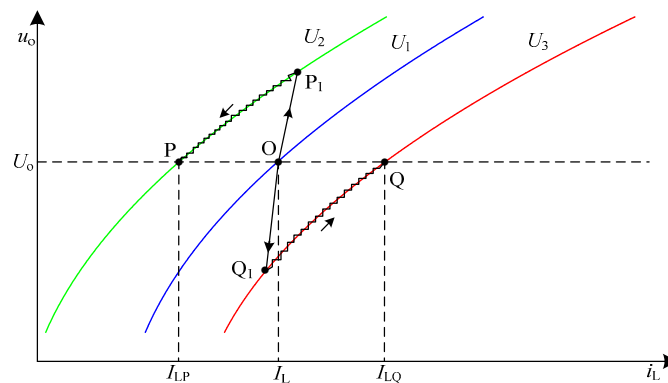


Figure 6. The transient trajectory in the i_L - u_o plane for input voltage perturbations.

3.2. Analysis of Transient Process under Load Perturbations

Figure 7 shows the transient trajectory of i_L and u_o under different load perturbations. When R decreases from R_0 to R_1 , the transient output power is larger than the input power, which results in u_o decreases and i_L increases. Therefore, (i_L, u_o) immediately move from the initial equilibrium operating point $O (I_L, U_o)$ to M_1 , then reach the new equilibrium operating point $M (I_{LM}, U_o)$ under the control of the sliding law of S_2 . A symmetrical situation will occur when load resistance R increases from R_0 to R_2 . As shown in the same figure, the correction effects make i_L equal to I_{LN} . Along the trajectory $O \rightarrow N_1 \rightarrow N$, (i_L, u_o) reach to the new equilibrium point $N (I_{LN}, U_o)$.

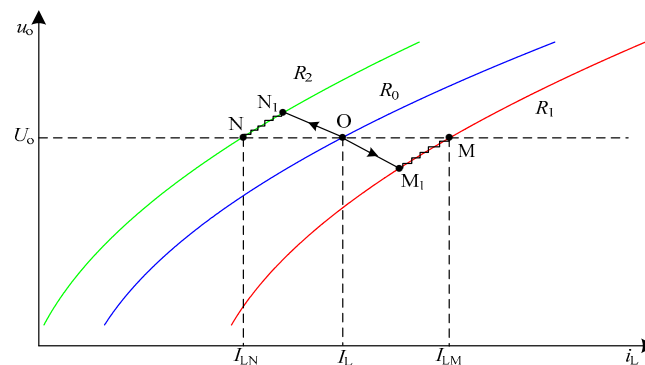


Figure 7. The transient trajectory in the i_L - u_o plane for load perturbations.

3.3. Simulation of the Sliding Control Based on S_2 in Steady-State

Figure 8 shows the simulation result of the transition between switching sliding function S_1 and S_2 when the u_o increases to U_o (24 V), there is only a small dynamic voltage deviation from U_o due to the PI regulator of u_o . As shown in Figure 8, the duration of the start-up is 13 ms. The ripple of u_o is less than 0.05 V.

Figure 9 shows the simulation response of the step perturbation superimposed on the input voltage. The nominal value of the input voltage is 12 V in Figure 9a. u_{in} is reduced from 12 V to 9 V at 0.15 s, which leads to a deviation of u_o . However, it only takes 22 ms for u_o to recover to nominal value due to the sliding mode control based on S_2 . Moreover, the maximum reduction value is only 1.28 V. Figure 9b also shows good dynamic and steady-state performance when u_{in} increases from 12 V to 15 V. The transient process is consistent with the (i_L, u_o) trajectory shown in Figure 6.

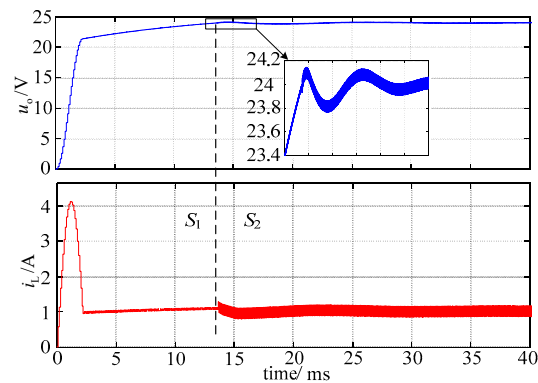


Figure 8. Simulation results of the transition between the two sliding functions.

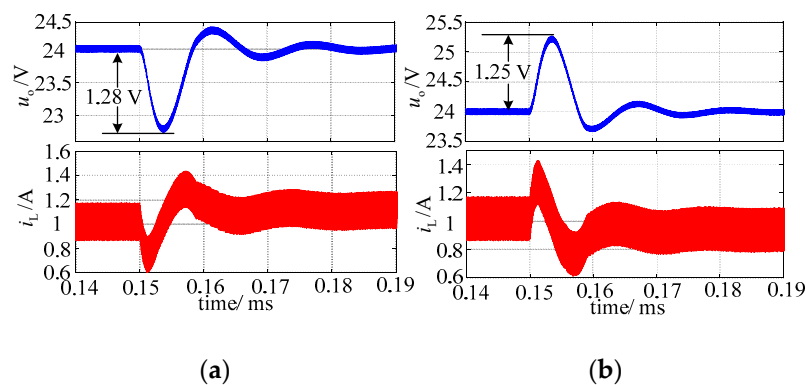


Figure 9. Simulation response to input voltage perturbations. (a) Reduction of u_{in} . (b) Increase of u_{in} .

Figure 10 shows the simulation responses of u_o and i_L under the perturbation of load from 40Ω to 50Ω and from 50Ω to 40Ω respectively. After a slight transient oscillation, u_o returned to the nominal value of 24 V. The maximum reduction value is 0.7 V and dynamic adjustment time is 15 ms. The transient process is consistent with the track of (i_L, u_o) shown in Figure 7.

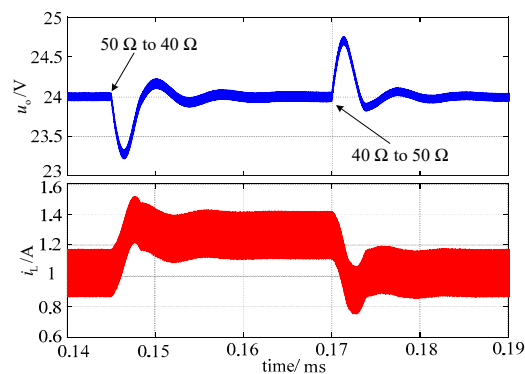


Figure 10. Simulation response to load perturbations.

4. Electronic Implementation Based on DSP

Figure 11 is a photograph of the boost converter experimental platform. In this platform for experimental verification, an oscilloscope is used to distinguish the voltage. The input voltage is supplied by a programmable power source. The type of DSP is TMS320F28335, which supports floating-point operation. The type of IGBT is PM400HSA120 and the type of diode is RM300HA-24F, which have a sample frequency up to 40 kHz.

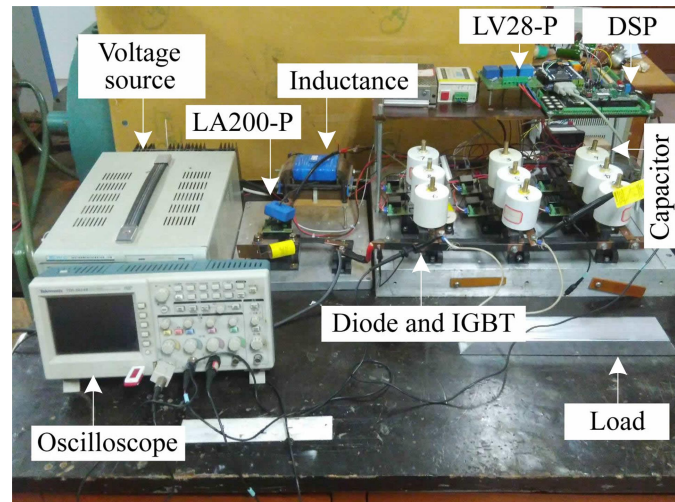


Figure 11. Picture of the experimental setup for the boost converter.

4.1. Detection and Conversion of Input Current and Output Voltage

Figure 12 shows the detection and filter circuit of i_L and u_o , current sensor (LA200-P) and voltage sensor (LV28-P) are adopted to detect i_L and u_o , respectively. The output current i_{IM} of LA200-P is proportional to i_L .

$$i_{IM} = k_1 i_L \tag{21}$$

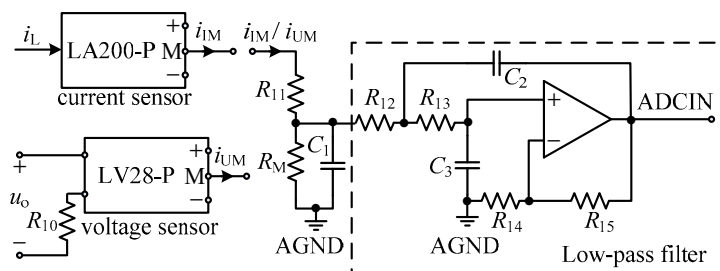


Figure 12. Detection and filter circuit of i_L and u_o .

k_1 , which is the conversion ratio of LA200-P, equal to 0.0005. For voltage detection, an input resistance R_{10} is used to convert the voltage to the primary current, so the relationship between the output current i_{UM} of LV28-P and u_o is

$$i_{UM} = k_2 u_o / R_{10}. \tag{22}$$

k_2 is the conversion ratio of LV28-P and equal to 2.5, then i_{UM} and i_{IM} generate voltage across the sample resistance R_M . Before enforcing A/D conversion by DSP, the voltage of R_M should be filtered by a low pass filter circuit with a bandwidth of 200 Hz.

Since the size of the result register in TMS28335 is 12-bits and the maximum conversion analog voltage is 3 V, the digital value (X_{IM}) of the result register used to obtain i_L can be expressed as:

$$X_{IM} = (2^{12} - 1) i_{IM} R_M / 3. \tag{23}$$

According to Equations (21) and (23), DSP can calculate i_L from X_{IM} by:

$$i_L = \frac{3 X_{IM}}{(2^{12} - 1) k_1 R_M}. \tag{24}$$

The calculation method of u_o from the digital value (X_{UM}) of result register is given directly:

$$u_o = \frac{3X_{IM}R_{10}}{(2^{12} - 1)k_2R_M}. \quad (25)$$

4.2. Software Implementation for Sliding Mode Control

The discrete program of sliding mode control based on S_1 and S_2 is enforced in the interrupt program caused by A/D conversion. A Boolean type variable flag is created to determine whether u_o is in the steady-state. If $\text{flag} = 0$, u_o is still in the start-up process, so the switching signal generated by the discrete program of sliding mode control is based on S_1 . Otherwise, S_2 is adopted to replace S_1 . The flow chart is shown in Figure 13.

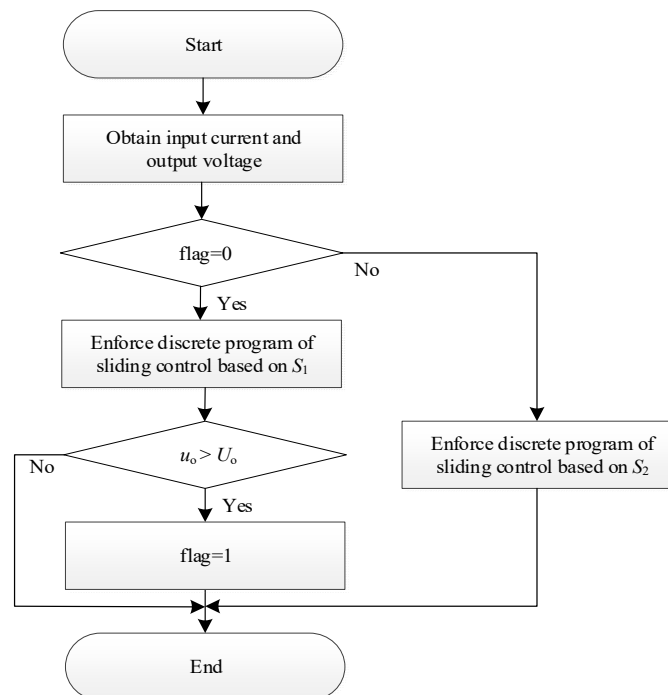


Figure 13. Interrupt program flow chart caused by A/D conversion.

5. Experimental Results

Figure 14 shows the experimental waveform of u_o from the zero initial-state to the steady-state. Compared to the results shown in Figure 4a, there is no overshoot of u_o in the start-up process under the effect of sliding mode control based on S_1 . When u_o first increases to 24 V, sliding mode control based on S_2 is adopted, the transition between switching surface S_1 and S_2 is in an agreement with the simulation results shown in Figure 8. As shown in this figure, good performance of the boost converter in the start-up process can be obtained by the switching surface S_1 . The duration of the start-up is 20 ms and the voltage overshoot is only 4.1%.

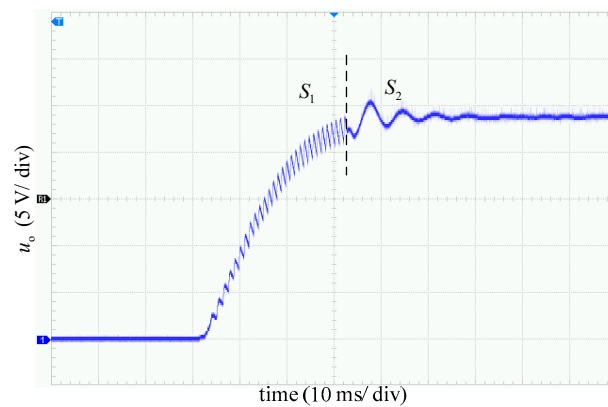


Figure 14. Experimental results from the zero steady-state to the steady-state.

Figure 15 illustrates the experimental response of the input voltage step decreasing from 12 V to 9 V. In contrast, Figure 16 illustrates the response of the input voltage, increasing from 12 V to 15 V. The experimental results are in good agreement with the simulation results shown in Figure 9. After ignoring the transient state, the action of the switching surface S_2 can realize a zero steady-state error of u_o . The maximum deviation value is 1.3 V and the dynamic adjustment time is less than 20 ms.

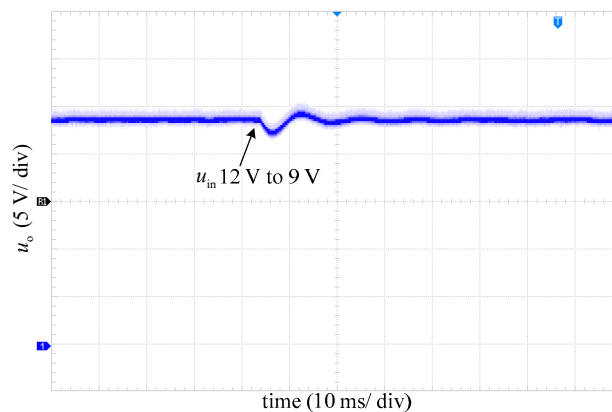


Figure 15. Experimental response of input voltage step increasing.

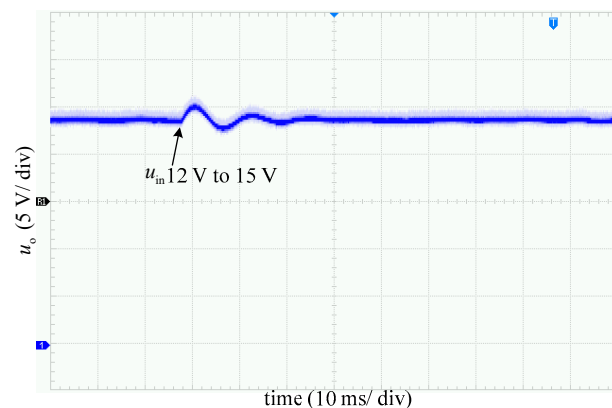


Figure 16. Experimental response of input voltage step decreasing.

Figure 17 shows the experimental response of the perturbation of load from 40 Ω to 50 Ω and from 50 Ω to 40 Ω respectively. A resistance of 200 Ω series connected with an auxiliary tube is parallel in the nominal load. The perturbation of load is achieved by controlling the auxiliary tube by the switching-on or switching-off state, the switching signal of the auxiliary tube is shown in Figure 17.

Under the action of the switching surface S_2 , A zero steady-state error of u_o is also achieved after ignoring the transient state. The maximum deviation value is 2.5 V and the dynamic adjustment time is less than 22 ms. The robustness is proved by simulation and experimental results.

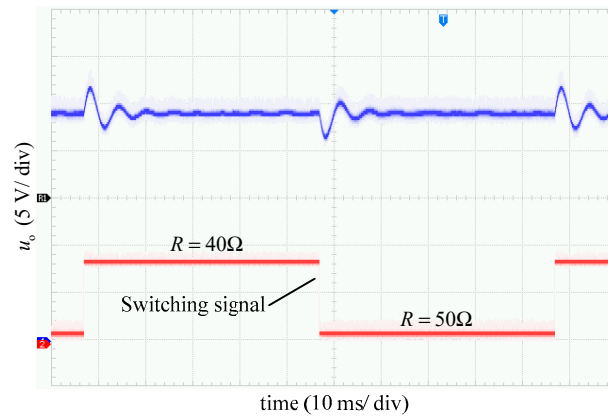


Figure 17. Experimental response to load perturbations.

6. Conclusions

For the different conditions of the start-up process and steady-state process of the boost converter, two switching surfaces are proposed in this paper respectively. In the start-up process of the boost converter, switching surface S_1 , which based on the large-signal model to minimize inrush current, voltage overshoot and adjustment time, is adopted. When the converter operates at a steady-state, the other switching surface S_2 including PI compensator is employed to regulate the output voltage, which can suppress the perturbation of input voltage and load fluctuation on the output voltage. Furthermore, the effectiveness of the control strategy proposed in this paper is verified by simulation and experiment. The research results can provide a reference for the engineering design of the sliding mode boost controller, so that the minimum value of the inrush current is compatible with the high voltage regulation value. In electric vehicle applications, the sliding mode control strategy proposed in this paper can be used in a boost converter between the battery and the inverter to suppress battery voltage fluctuations and improve system efficiency.

Author Contributions: Investigation, T.Y.; Software, T.Y.; Writing—original draft preparation, T.Y.; Writing—review and editing, T.Y. and Y.L.

Funding: This research received no external funding.

Conflicts of Interest: The authors declare no conflict of interest.

References

1. He, J.P.; Jun, Y.; Gong, B.; Lei, J.S.; Liu, Y.; Long, F. Analysis of start-up inrush current and its mitigation control strategy for grid connected voltage source inverter. In Proceedings of the 2014 IEEE Conference and Expo Transportation Electrification Asia-Pacific (ITEC Asia-Pacific), Beijing, China, 31 August–3 September 2014; pp. 1–4.
2. Wu, Y.; Huangfu, Y.; Zhang, L.; Zhou, L. A Robust High Order Sliding Mode for Buck-Boost Converters With Large Disturbances. *Proc. CSEE* **2015**, *35*, 1740–1748.
3. Wang, Y.X.; Yu, D.H.; Kim, Y.B. Robust time-delay control for the DC–DC Boost Converter. *IEEE Trans. Ind. Electron.* **2014**, *61*, 4829–4837. [[CrossRef](#)]
4. Barhoumi, E.M.; Belgacem, I.B.; Khiareddine, A.; Zghaibeh, M.; Tlili, I. A Neural Network-Based Four Phases Interleaved Boost Converter for Fuel Cell System Applications. *Energies* **2018**, *11*, 3423. [[CrossRef](#)]
5. Rodič, M.; Milanović, M.; Truntič, M.; Ošljaj, B. Switched-Capacitor boost converter for low power energy harvesting applications. *Energies* **2018**, *11*, 3156. [[CrossRef](#)]

6. Baždarić, R.; Vončina, D.; Škrjanc, I. Comparison of novel approaches to the predictive control of a DC-DC boost converter based on heuristics. *Energies* **2018**, *11*, 3300. [[CrossRef](#)]
7. Bai, H.; Mi, C.T.; Wang, C.W.; Gargies, S. The dynamic model and hybrid phase-shift control of a dual-active-bridge converter. In Proceedings of the 34th Annual Conference of IEEE Industrial Electronics, Orlando, FL, USA, 10–13 November 2008; pp. 2840–2845.
8. Su, J.H.; Chen, J.J.; Wu, D.S. Learning feedback controller design of switching converters via MATLAB/SIMULINK. *IEEE Trans. Educ.* **2002**, *45*, 307–315.
9. Sreekumar, C.; Agarwal, V. A hybrid control algorithm for voltage regulation in DC–DC Boost Converter. *IEEE Trans. Ind. Electron.* **2008**, *55*, 2530–2538. [[CrossRef](#)]
10. Anzehaee, M.M.; Behzad, B.; Hajihosseini, P. Augmenting ARMarkov-PFC predictive controller with PID-Type III to improve boost converter operation. *Control Eng. Pract.* **2018**, *79*, 65–77. [[CrossRef](#)]
11. Chan, C.Y. A Nonlinear Control for DC-DC Power Converters. *IEEE Trans. Power Electron.* **2007**, *22*, 216–222. [[CrossRef](#)]
12. Martínez-Salamero, L.; García, G.; Orellana, M.; Lahore, C.; Estibals, B.; Alonso, C.; Carrejo, C.E. Analysis and design of a sliding-mode strategy for start-up control and voltage regulation in a buck converter. *IET Power Electron.* **2013**, *6*, 52–59. [[CrossRef](#)]
13. RakhtAla, S.M.; Yasoubi, M.; HosseinNia, H. Design of second order sliding mode and sliding mode algorithms: A practical insight to DC-DC buck converter. *IEEE/CAA J. Autom. Sin.* **2017**, *4*, 483–497. [[CrossRef](#)]
14. Lai, N.O.; Edwards, C.; Spurgeon, S.K. On output tracking using dynamic output feedback discrete-time sliding-mode controllers. *IEEE Trans. Autom. Control* **2007**, *52*, 1975–1981. [[CrossRef](#)]
15. Yang, H.T.; Zhang, Y.C.; Liang, J.J.Y.; Gao, J.H.; Walker, P.D.; Zhang, N. Sliding-Mode observer based voltage-sensorless model predictive power control of PWM rectifier under unbalanced grid conditions. *IEEE Trans. Ind. Electron.* **2018**, *65*, 5550–5560. [[CrossRef](#)]
16. Kim, J.K.; Ko, J.S.; Lee, J.; Lee, Y. Rotor flux and rotor resistance estimation using extended Luenberger-Sliding mode observer (ELSMO) for three phase induction motor control. *Can. J. Electr. Comput. Eng.* **2017**, *40*, 181–188.
17. Yang, C.Y.; Ma, T.T.; Che, Z.; Zhou, L. An adaptive-gain sliding mode observer for sensorless control of permanent magnet linear synchronous motors. *IEEE Access* **2018**, *6*, 3469–3478. [[CrossRef](#)]
18. Montoya, D.G.; Ramos-Paja, C.A.; Giral, R. Improved design of sliding-mode controllers based on the requirements of MPPT techniques. *IEEE Trans. Power Electron.* **2016**, *31*, 235–247. [[CrossRef](#)]
19. Chincholkar, S.H.; Chan, C.Y. Design of fixed-frequency pulsewidth-modulation-based sliding-mode controllers for the quadratic boost converter. *IEEE Trans. Circuits Syst. II Express Briefs* **2017**, *64*, 51–55. [[CrossRef](#)]
20. Mademlis, G.; Steinke, G.K.; Rufer, A. Feed-Forward-Based control in a DC–DC converter of asymmetric multistage-stacked boost architecture. *IEEE Trans. Power Electron.* **2017**, *32*, 1507–1517. [[CrossRef](#)]
21. Singh, S.; Fulwani, D.; Kumar, V. Robust sliding-mode control of dc/dc boost converter feeding a constant power load. *IET Power Electron.* **2015**, *8*, 1230–1237. [[CrossRef](#)]
22. Chen, Y.; Nan, Y.R.; Kong, Q.G.; Zhong, S. An Input-Adaptive Self-Oscillating Boost Converter for Fault-Tolerant LED Driving with Wide-Range Ultralow Voltage Input. *IEEE Trans. Power Electron.* **2015**, *30*, 2743–2752. [[CrossRef](#)]
23. Martínez-Treviño, B.A.; Aroudi, A.E.; Martínez-Salamero, L. Sliding-mode approach for start-up control and voltage regulation of a boost converter driving a constant power load. In Proceedings of the 2017 IEEE International Symposium on Circuits and Systems (ISCAS), Baltimore, MD, USA, 28–31 May 2017.
24. Martínez-Salamero, L.; García, G.; Orellana, M.; Lahore, C.; Estibals, B. Start-Up control and voltage regulation in a boost converter under sliding-mode operation. *IEEE Trans. Ind. Electron.* **2013**, *60*, 4637–4649. [[CrossRef](#)]

